Morphology-based segmentation of newborn brain MR images

Laura Gui[1], Radoslaw Lisowski[2], Tamara Faundez[3], Petra S. Hüppi[3], François Lazeyras[2], and Michel Kocher[4]

[1] Faculty of Medicine, University of Geneva, Geneva, Switzerland
[2] Department of Radiology and Medical Informatics, University of Geneva, Geneva, Switzerland
[3] Department of Pediatrics, Geneva University Hospitals, Geneva, Switzerland
[4] Biomedical Imaging Group, Ecole Polytechnique Fédérale de Lausanne, Lausanne, Switzerland

Abstract. We present an algorithm for the segmentation of newborn brain MR images, relying on high-level brain morphology knowledge, concerning relative tissue location, connectivity and structure. Our method is fully automatic and does not require the use of any atlas or template. The use of widely- recognized assumptions regarding neonatal brain morphology makes the method applicable to different neonatal populations, while avoiding atlas-related bias. The algorithm segments the brain both globally (intracranial cavity, cerebellum, brainstem and the two hemispheres) and at tissue level (cortical and subcortical gray matter, myelinated and unmyelinated white matter, and cerebrospinal fluid). Visual inspection and quantitative comparisons show good agreement of the segmentation results with expert manual segmentations.

1 Introduction

The segmentation of neonatal brain MR images is a primary step in the study of neonatal brain development. Compared to the segmentation of adult brain MRI, it faces a number of additional challenges, requiring the development of dedicated algorithms: the lower signal-to-noise ratios and stronger partial volume effects (due to smaller brain size and limited acquisition time), as well as the reduced and inverted image contrast, due to ongoing white matter myelination.

Recent years have seen significant advances in newborn brain segmentation. Some authors used manual voxel selection/segmentation to obtain training data for k-nearest neighbors (KNN) classification schemes integrating intensity data and spatial priors given by templates [13] or training voxel coordinates [1]. Weisenfeld and Warfield [14] used a library of template subjects with manually-selected tissue class prototypes, which they projected onto the target subject to learn tissue class probabilities. This generated segmentations of the target subject corresponding to each template subject, that were fused into a consensus segmentation, refined by pruning out inconsistent prototypes, and reiterating the process. Alternatively to manual selection, tissue intensity models

were derived through unsupervised learning techniques, implemented via EM algorithms. Some authors enhanced classic EM schemes for adult brain segmentation by introducing robust graph clustering for tissue model estimation [9], or a dedicated CSF/gray matter partial-volume removal step [15]. Shi et al. [10] used segmentations of better-contrasted later-age scans of their subjects' as priors for the segmentation of corresponding neonatal scans. Wang et al. [12] used the atlas of [11] in a coupled level-set segmentation with a cortical thickness constraint. Coupled surface evolution is also used by [5] in an atlas-free approach based on local image contrast and geometrical features.

Most authors deal with the challenges of neonatal brain segmentation by introducing strong prior knowledge into the segmentation schemes (atlases or manually selected prototypes). Such prior knowledge is population-dependent and its application risks eliminating differences among populations that one might want to investigate. We propose a different approach to neonatal brain segmentation, based on the use of widely-accepted knowledge of neonatal brain morphology, regarding tissue connectivity, structure and relative positions. For instance, we use the information that the white matter is a connected tissue, surrounded by cortical gray matter, which is surrounded by extra-ventricular CSF. This information is introduced in the form of neighborhood selection criteria for a region growing algorithm separating white matter, gray matter and CSF, to avoid partial volume errors at the gray matter/CSF interface. Similarly, each step of our algorithm is based on well-established segmentation techniques, where we apply specifically designed segmentation functions incapsulating high-level brain morphology knowledge. The use of such high-level knowledge ensures our method's generality and widespread applicability to different newborn populations. Our algorithm performs a comprehensive segmentation of the newborn brain into large-scale structures (the two hemispheres, the cerebellum and the brainstem), and fine-scale structures (the cortical and the subcortical gray matter, the myelinated and the unmyelinated white matter and the CSF). Segmentation accuracy is confirmed by visual inspection and by quantitive comparisons with manual segmentations.

2 METHOD

The proposed segmentation algorithm consists of five steps: extraction of the intracranial cavity (ICC) and of the two hemispheres, detection of the subcortical gray matter (SGM), separation of the cortical gray matter (CGM), unmyelinated white matter (UWM) and CSF, segmentation of the cerebellum and of the brainstem, and detection of the myelinated white matter (MWM). The input data for our algorithm consists of T1 and T2 MR scans of a newborn brain of gestational age (GA) between 38 and 44 weeks. Before segmentation, we apply standard preprocessing steps: intensity inhomogeneity correction [8], rigid registration of the T2 image to the T1 image [7], alignment to the radiological orientation, resampling to obtain isotropic voxels, and anisotropic diffusion filter to reduce noise while preserving edges [4].

2.1 Intracranial Cavity Extraction and Hemisphere Separation

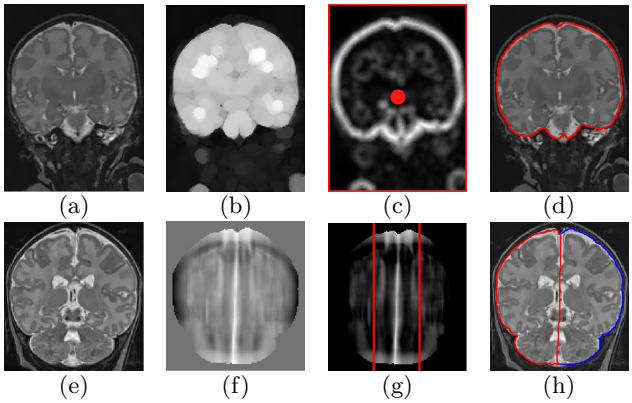

Fig. 1. ICC extraction (a-d) and hemisphere separation (e-h). (a) Filtered T2 image; (b) opening of (a); (c) segmentation function with internal and external markers (in red); (d) ICC watershed segmentation; (e) filtered T2 image; (f) symmetry function; (g) segmentation function with markers; (h) watershed segmentation of the hemispheres.

ICC extraction is performed with the marker-based watershed algorithm [2], using the knowledge that the ICC is a connected volume, and its border with the skull is marked by a strong edge on the T2 image. We perform an opening of the T2 image (Fig. 1(b)) and compute its morphological gradient. The segmentation function is given by the sum of increasing scale dilations of the gradient (Fig. 1(c)). The internal marker is a small sphere around the gravity center of the head mask, obtained by T2 image thresholding. The external marker is the T2 image bounding box. Watershed segmentation yields the contour from Fig. 1(d).

Next, we employ the marker-based watershed to separate the hemispheres, with a segmentation function exploiting their symmetry. Namely, we use the correlation coefficient at each voxel between a small T2 image cuboid centered on the voxel and its left-right (x axis) flip: $\rho_{uu'} = \sigma_{uu'}/\sqrt{\sigma_{uu}\,\sigma_{u'u'}}$, with u and u' the vectorized volumes, and $\sigma_{uu'}$ their covariance (Fig. 1(f)). Being interested in positive correlation, we set the function to zero in locations with negative correlation coefficients (Fig. 1(g)). Hemisphere markers are two sagittal planes equally distanced on the x axis with respect to the ICC gravity center (Fig. 1(g)). Hemisphere segmentation results are presented in Fig. 1(h).

2.2 Subcortical gray matter detection

SGM has similar intensity to CGM, but can be distinguished from it based on its relatively compact structure. Morphological closing of the T2 image is used to lighten fine dark regions of CGM, while preserving large dark regions of SGM. We compute the sum of increasing scale closings of the filtered T2 image and use it as a segmentation function for similarity-based watershed segmentation [6] (Fig. 2(b)). For the markers, we use a large scale closing of the T2 image (Fig. 2(c)). We determine its regional minima and, for each hemisphere, we

choose as a marker the regional minimum of highest volume dynamics. The external marker is the ICC border. The segmentation result is presented in Fig. 2(d).

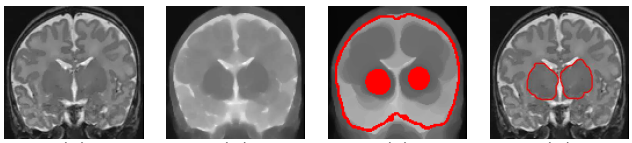

(a) (b) (c) (d)

Fig. 2. Subcortical gray matter detection. (a) Filtered T2 image; (b) segmentation function (sum of increasing scale closings of (a)); (c) markers superposed on large scale closing of (a); (d) SGM segmented by similarity-based watershed.

2.3 Detection of the cortical gray matter, of the unmyelinated white matter and of the CSF

To cope with partial volume effects at the interface between the CGM and the CSF, we use region growing segmentation and impose anatomical-based conditions on voxel neighborhood. During region growing, we discriminate between ventricular CSF and CSF surrounding the cortex (external CSF), which allows us to use the knowledge that UWM cannot be found in the neighborhood of external CSF. Region growing is limited to the ICC, excluding SGM. The algorithm features three regions growing: UWM, ventricular CSF and external CSF. The CGM is obtained as the complement of these regions with respect to the growth area. To obtain seeds for the growing regions (Fig. 3(d)), we perform k-means classification of T2 image values in three classes: CGM, UWM and CSF (Fig. 3(c)). We perform an opening of the UWM and take the largest connected component (LCC) in each hemisphere as UWM seed. Ventricular CSF seeds are the CSF voxels neighboring SGM. External CSF seeds are the CSF or background voxels neighboring the ICC border.

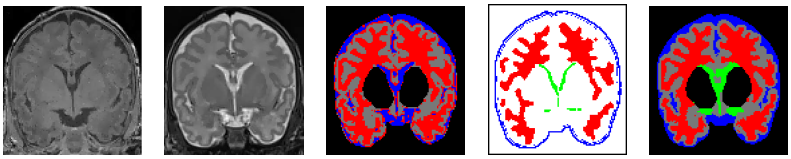

(a) (b) (c) (d) (e)

Fig. 3. Detection of cortical gray matter, unmyelinated white matter and CSF. (a) Filtered T1 image; (b) filtered T2 image; (c) k-means classification ($k = 3$) of T2 image growth region; (d) region seeds; (e) region growing result. Legend: gray - CGM, red - UWM, blue - external CSF, green - ventricular CSF.

As metric we use the Mahalanobis distance with respect to a set of tissue representative feature vectors: $d_M(u, V) = \sqrt{(u - \mu_V)^\top \Sigma_V^{-1} (u - \mu_V)}$, where $u = (u_1, u_2)^\top$ contains T1 and T2 voxel intensities, V is a matrix whose columns

are the tissue representative feature vectors, and μ_V and Σ_V are the mean and covariance, respectively, of the vectors in V. Representative feature vectors for each tissue belong to the corresponding voxels resulted from k-means classification. Starting from each tissue's seeds, we select candidates among its unlabeled neighbors, such that their Mahalanobis distance to the tissue is smaller than the one to the CGM, and they obey a set of neighborhood restrictions. For UWM, candidates exclude external CSF and background voxel neighbors; for external CSF, they exclude UWM and SGM neighbors. Then, we compute the median of the candidates' Mahalanobis distance to their corresponding tissue. We select the tissue of minimum median distance and expand it by adding all its candidates whose Mahalanobis distance is smaller or equal to the median. Next, we re-compute tissue candidates and iterate the process until no voxels can be added to any tissue. Classification results can be seen in Fig. 3(e).

2.4 Detection of the cerebellum and of the brainstem

The detection of the cerebellum and of the brainstem is performed in two steps: separation of the whole cerebellum region from the cerebrum, and classification into cerebellum, brainstem and CSF.

Fig. 4. Cerebellum region segmentation. (a) Unfiltered T2 image; (b) segmentation function given by sum of increasing scale dilations of (a); (c) union of UWM and SGM, refined by opening and LCC selection in each hemisphere; contour is rough cerebrum outline obtained via dilation and closing of union; (d) cerebrum (green) and cerebellum (red) markers; (e) watershed cerebellum region segmentation.

Segmentation of the cerebellum region We exploit the knowledge that there is a fine layer of CSF between the cerebellum and the cerebrum (Fig. 4(a)). We emphasize this separating layer by computing a segmentation function given by the sum of increasing scale dilations of the unfiltered T2 image, with the background set to the maximum T2 image intensity (Fig. 4(b)). For the cerebrum marker, we derive a rough mask of the cerebrum (Fig. 4(c), green) by dilation and closing of the union of UWM and SGM, refined via opening and LCC selection in each hemisphere (Fig. 4(c), white). The cerebrum marker is an erosion of the rough cerebrum mask (Fig. 4(d), green). For the cerebellum marker, we select CGM voxels not included in the rough cerebrum mask, and perform an opening, followed by erosion (Fig. 4(d), red). Then, we detect the cerebellum region via marker-based watershed segmentation (Fig. 4(e)).

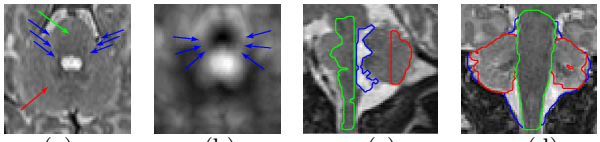

(a) (b) (c) (d)

Fig. 5. Separation of cerebellum and brainstem. Axial slices of (a) unfiltered T2 image; blue arrows indicate CSF separating cerebellum (red arrow) from brainstem (green arrow); (b) sum of increasing scale dilations of (a); (c) Sagittal T2 slice, with brainstem and cerebellum markers and fourth ventricle CSF. (d) Coronal slice with watershed segmentation refined by CSF removal. Brainstem - green, cerebellum - red, CSF - blue.

Separation of cerebellum and brainstem We use CSF regions to separate cerebellum and brainstem. We build a segmentation function for the marker-based watershed by computing the sum of increasing scale dilations of the T2 image, to create bridges between fragmented CSF regions (Fig. 5(b)). For the markers, we perform k-means classification of the filtered T2 image values from the cerebellum region in 3 classes: gray matter (GM), white matter (WM) and CSF. Then, we determine two anatomic landmarks: the fourth CSF ventricle, given by CSF voxels belonging to a closing of GM and WM, and a thick inter-hemispheric band, obtained by dilating the inter-hemispheric separation. The cerebellum marker is given by GM voxels posterior to the fourth ventricle, while the brainstem marker is given by GM voxels from the inter-hemispheric band situated anterior to the fourth ventricle (Fig. 5(c)). Marker-based watershed separates the brainstem and cerebellum regions, which are then refined by eliminating k-means detected CSF(Fig. 5(d)).

2.5 Detection of the myelinated white matter

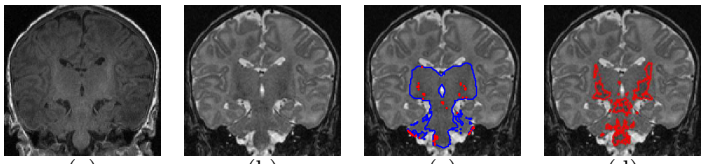

(a) (b) (c) (d)

Fig. 6. Myelinated white matter detection. Unfiltered T1 (a) and T2 (b) images; (c) T2 image with contours of the target regions (blue) and the segmentation initialization (red); (d) final myelin region.

To determine MWM within the brain of a newborn from our target age interval (38 to 44 weeks GA at scan time), we focus on the target regions most likely to contain myelin at this age: the SGM, the brainstem and the GM areas detected in the cerebellum classification (Fig. 6(c), blue). We use 3D region-based active contour segmentation [3], constraining the segmentation within the target regions. The inputs are the unfiltered T1 and T2 images (Fig. 6(a, b)), and the initial region is set to contain the 1% highest intensity T1 image voxels from the target regions (Fig. 6(c), red). Then, we deform the initial region within the target regions to separate myelin from other tissues based on their different mean intensity (lower T2, higher T1) - Fig. 6(d)).

3 Results and conclusion

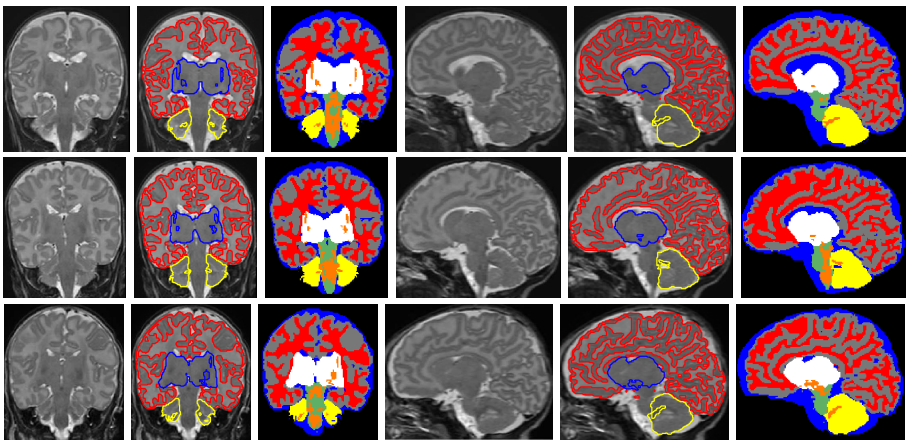

Fig. 7. Segmentation results. Each row corresponds to a different subject and contains 3 coronal slices and 3 axial slices of the T2 image, the T2 image with contours of the CGM (red), SGM (blue) and cerebellum (yellow), and the segmentation labels: gray - CGM, white - SGM, red - UWM, orange - MWM, yellow - cerebellum, green - brain stem (unmyelinated).

Table 1. Dice similarity coefficient (DC) and 95th-percentile Hausdorff distance (HD) between the proposed segmentation and the manual standard segmentation. Bm - brainstem, Cb - cerebellum.

Subj.	CGM		UWM		SGM		Bm		Cb		CSF	
	DC	HD	DC	HD	DC	HD	DC	HD	DC	HD	DC	HD
1	0.74	0.79	0.90	0.50	0.88	0.79	0.69	1.57	0.88	0.79	0.75	2.43
2	0.76	0.99	0.87	0.70	0.85	1.25	0.71	2.16	0.90	0.70	0.72	2.13
3	0.78	0.70	0.90	0.50	0.83	1.43	0.74	1.76	0.90	0.70	0.67	2.78

We tested our algorithm on three newborn brains of 40 weeks GA provided for the MICCAI NeoBrainS12 challenge, acquired as follows: coronal 3D T1-weighted images TR=9.5 ms; TE=4.6 ms; reconstruction matrix=256x256; number of sections=110, resolution 0.78 mm x 0.78 mm x 1.2 mm; coronal T2-weighted images TR=4847 ms; TE=150 ms; reconstruction matrix=512x512; number of sections=110, resolution 0.35 mm x 0.35 mm x 1.2 mm. Our algorithm's run-time was around 2 hours per brain on a 3.06 GHz iMac with an Intel Core 2 Duo processor.

Segmentation accuracy was confirmed by visual inspection of medical experts. Our algorithm is able to capture the fine structure of CGM, and is robust against partial volume errors at the CSF/CGM interface. Table 1 presents the quantitative evaluation of the method with respect to a manual standard segmentation using the Dice coefficient and 95th-percentile Hausdorff distance. Since most of the brainstem is myelinated tissue, its voxels should carry a double label: myelin and brainstem. Quantitative evaluation was only possible for a unique label per voxel, therefore we evaluated the segmentation results without myelin (as ob-

tained before the last step of our pipeline). For most tissues and subjects the Dice coefficients are greater than 0.7, indicating good agreement.

To conclude, we proposed a segmentation algorithm for newborn brain MRI, based on high-level knowledge of neonatal brain morphology. Our algorithm does not require manual intervention, and does not utilize a brain atlas or template. It is able to distinguish a complete set of brain structures essential for the assessment of brain development at the neonatal age, namely the hemispheres, the cerebellum and the brainstem, cortical and subcortical gray matter, myelinated and unmyelinated white matter and CSF. Experimental results are visually accurate and show good overlap with manual segmentations.

References

1. Anbeek, P., Vincken, K.L., Groenendaal, F., Koeman, A., van Osch, M.J.P., van der Grond, J.: Probabilistic brain tissue segmentation in neonatal magnetic resonance imaging. Pedriatric Research 63(2), 158–163 (2008)
2. Beucher, S., Meyer, F.: The morphological approach to segmentation: the watershed transformation. In: Dougherty, E.R. (ed.) Mathematical Morphology in Image Processing, pp. 433–481. CRC Press, New York (1993)
3. Chan, T.F., Sandberg, Y.B.: Active contours without edges for vector valued image. Journal of Visual Communication and Image Representation 11, 130–141 (2000)
4. Gerig, G., Kübler, O., Kikinis, R., Jolesz, F.: Nonlinear anisotropic filtering of MRI data. IEEE Trans. Med. Imaging 11(2), 221–232 (1992)
5. Leroy, F., Mangin, J.F., Rousseau, F., Glasel, H., Hertz-Pannier, L., Dubois, J., Dehaene-Lambertz, G.: Atlas-free surface reconstruction of the cortical grey-white interface in infants. PLoS ONE 6(11), e27128 (2011)
6. Lotufo, R., Falcão, A.: The ordered queue and the optimality of the watershed approaches. In: Mathematical Morphology and its Application to Image and Signal Processing. Kluwer Academic Publishers (2000)
7. Maes, F., Collignon, A., Vandermeulen, D., Marchal, G., Suetens, P.: Multimodality image registration by maximization of mutual information. IEEE Trans. Pattern Analysis and Machine Intelligence 16(2), 187–198 (1997)
8. Mangin, J.F.: Entropy minimization for automatic correction of intensity nonuniformity. In: IEEE Workshop MMBIA. pp. 162–169 (2000)
9. Prastawa, M., Gilmore, J.H., Lin, W., Gerig, G.: Automatic segmentation of MR images of the developing newborn brain. Med. Image Anal. 9(5), 457–466 (2005)
10. Shi, F., Fan, Y., Tang, S., Gilmore, J.H., Lin, W., Shen, D.: Neonatal brain image segmentation in longitudinal MRI studies. Neuroimage 49, 391–400 (2010)
11. Shi, F., Yap, P.T., Wu, G., Jia, H., Gilmore, J.H., Lin, W., Shen, D.: Infant brain atlases from neonates to 1- and 2-year-olds. PLoS ONE 6(4), e18746 (2011)
12. Wang, L., Shi, F., Lin, W., Gilmore, J.H., Shen, D.: Automatic segmentation of neonatal images using convex optimization and coupled level sets. Neuroimage 58, 805–817 (2011)
13. Warfield, S.K., Kaus, M., Jolesz, F.A., Kikinis, R.: Adaptive, template moderated, spatially varying statistical classification. Med. Image Anal. 4(1), 43–55 (2000)
14. Weisenfeld, N.I., Warfield, S.K.: Automatic segmentation of newborn brain MRI. Neuroimage 47, 564–572 (2009)
15. Xue, H., Srinivasan, L., Jiang, S., Rutherford, M., Edwards, A.D., Rueckert, D., Hajnal, J.V.: Automatic segmentation and reconstruction of the cortex from neonatal MRI. Neuroimage 38(3), 461–477 (2007)